IJST, Transactions of Mechanical Engineering, Vol. 36, No. M2, pp 129-141
Printed in The Islamic Republic of Iran, 2012

THREE-DIMENSIONAL COMPUTATIONAL FLUID DYNAMIC STUDY ON PERFORMANCE OF POLYMER EXCHANGE MEMBRANE FUEL CELL (PEMFC) IN DIFFERENT CELL POTENTIAL *

N. AHMADI**, N. POURMAHMOUD, I. MIRZAEE AND S. REZAZADEH

Dept. of Mechanical Engineering, Urmia University of Technology, Urmia, I. R. of Iran
Email: nima.ahmadi.eng@gmail.com

Abstract– A full three-dimensional, single phase computational fluid dynamics model of a proton exchange membrane fuel cell (PEMFC) with both the gas distribution flow channels and the Membrane Electrode Assembly (MEA) has been developed. A single set of conservation equations which are valid for the flow channels, gas-diffusion electrodes, catalyst layers, and the membrane region are developed and numerically solved using a finite volume based computational fluid dynamics technique. In this research, some important parameters such as variation of oxygen and water mass fraction, liquid water activity and the membrane protonic conductivity have been presented at the entry and exit regions of the cell. The numerical results indicated that, at lower cell voltage (0.6v) which corresponds to higher current density, the hydrogen and oxygen consumption and, accordingly water production is high. Finally the numerical results of the proposed CFD model are compared with the available experimental data that represent good agreement.

Keywords– PEM fuel cells, cell potential, current density, CFD, fuel cell performance

1. INTRODUCTION

The proton exchange membrane fuel cell (PEMFC) using very thin polymer membrane as electrolyte has been considered as a promising candidate of future power sources, especially for transportation applications and residential power. This type of fuel cell has many important advantages such as high efficiency, clean, quiet, low temperature operation, capable of quick start-up, no liquid electrolyte and simple cell design. However, its performance and cost should be further optimized before this system becomes competitive with the traditional combustion power plants [1-4].

In recent years, research and development in fuel cells and fuel cell systems has increased; but at present, the cost of fuel cell systems is still too high for them to become viable commercial products.

In a fuel cell, fuel (e.g., hydrogen gas) and an oxidant (e.g., oxygen gas from the air) are used to generate electricity, while heat and water are typical products of the fuel cell operation. A fuel cell typically works on the following principle: as the hydrogen gas flows into the fuel cell on the anode side, a platinum catalyst facilitates oxidation of the hydrogen gas which produces protons (hydrogen ions) and electrons. The hydrogen ions diffuse through a membrane (the center of the fuel cell which separates the anode and the cathode); and again with the help of a platinum catalyst, combine with oxygen and electrons on the cathode side in order to produce water. The electrons, which cannot pass through the membrane, flow from the anode to the cathode through an external electrical circuit containing a motor or other electric system.

*Received by the editors June 28, 2011; Accepted June 20, 2012.
**Corresponding author

Both the anode and cathode (the electrodes) are porous and are made from an electrically conductive material, typically carbon. The faces of the electrodes are in contact with the membrane and contain carbon, polymer electrolyte and a platinum-based catalyst. Oxidation and reduction fuel-cell half reactions take place in the anode and the cathode active layer, respectively. The PEM electrodes are of gas-diffusion type and are generally designed for maximum surface area per unit material volume (the specific surface area). In this way gas diffusion layer can be available for the reactions in order to minimize transport resistance of the hydrogen and the oxygen to the active layers. In addition, it can be interpreted as easy removal of the water from the cathodic active layer and the minimum transport resistance of the protons from the active sites in the anodic layer to the active sites in the cathodic active layer.

Extensive research efforts have been devoted to developing realistic simulation models in the past decade. Researchers all over the world are focusing on optimizing the fuel cell system to be cost competitive with currently available energy conversion devices [5].

Many studies have examined various aspects of PEMFC performance as a function of operating conditions (e.g. [6–14]). One important tool in the optimization study of fuel cell performance is computational modeling, which can be used to reveal the fundamental phenomena taking place in the fuel cell system [15].

A great number of researches have been conducted to improve the performance of the PEMFC so that it can reach a significant market penetration. The performance of PEM fuel cells is known to be influenced by many parameters, such as operating temperature, pressure, humidification of the gas streams and geometrical parameters. Among the various aspects of PEMFCs that affect cell performance, geometrical parameters play a major role. For example, performance of the fuel cell with smaller shoulder widths is better than those with larger ones [16–19].

Effect of gas channel geometry on the performance of proton exchange membrane fuel cells was developed to investigate its performance. Two geometries with rectangular and trapezoidal channel configuration were simulated and the obtained results in a low cell voltage (which leads to high current densities in two geometries) were compared [20]. Pourmahmoud, et al. investigated the gas diffusion layer thickness effect on PEMFC performance [21]. Ahmadi et al studied the effect of parallelogram gas channel and shoulder geometry on fuel cell performance [22]. Ahmed and Sung [23] performed simulations of PEMFCs with a new design for the channel shoulder geometry.

In the present investigation, a three-dimensional, single phase, non-isothermal and parallel flow model of a PEM fuel cell with conventional and deflected membrane electrode assembly (MEA) have been simulated numerically, which incorporates the key parameters affecting fuel cell performance. Humidified hydrogen was used on the anode side, and then air was applied on the cathode side. A series of polarization curves with different deflections are obtained and represented. These curves show the trend of the PEM fuel cell performance with different deflections. The available experimental data are used in order to validate the results of polarization curve. The studied model is modified and used to study the effects of deflected MEA and several operating conditions on fuel cell characteristics. Detailed analyses of the fuel cell behavior under various deflection values are to be discussed in the following sections. In this research, some important parameters such as variation of oxygen and water mass fraction, liquid water activity and the membrane protonic conductivity have been presented at the entry and exit regions of the cell. The numerical results indicated that, at lower cell voltage (0.6v) which corresponds to higher current density, the hydrogen and oxygen consumption and, accordingly, water production is high.

2. MATHEMATICAL MODEL

In the present study, computational domain and its cross-sectional view are shown in Fig. 1 and 2. Also, the three dimensional structured grid of a cell is presented in Fig. 3. The cell consists of hydrogen and oxygen channels, bipolar plates on the cathode and anode side of the cell and the membrane electrode assembly (MEA) is located between the gas channels.

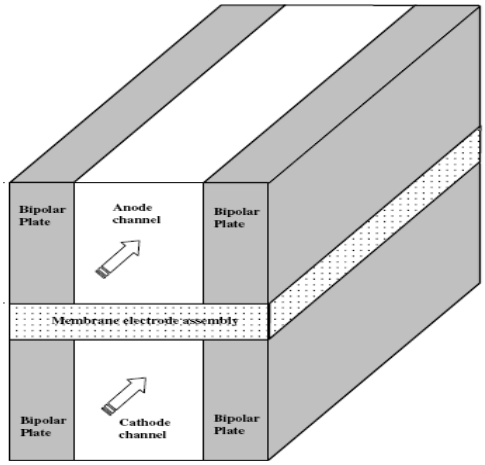

Fig.1. 3D schematic of a single straight-channel of PEMFC

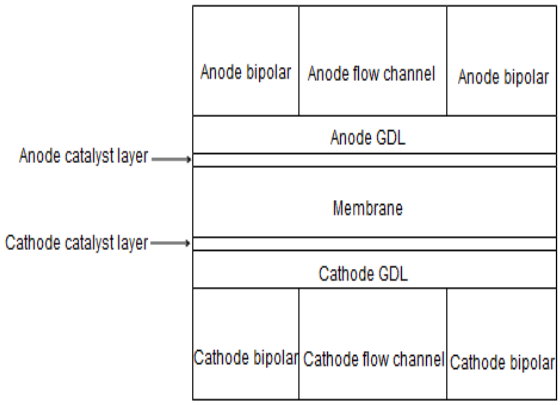

Fig. 2. 2D side view of PEMFC

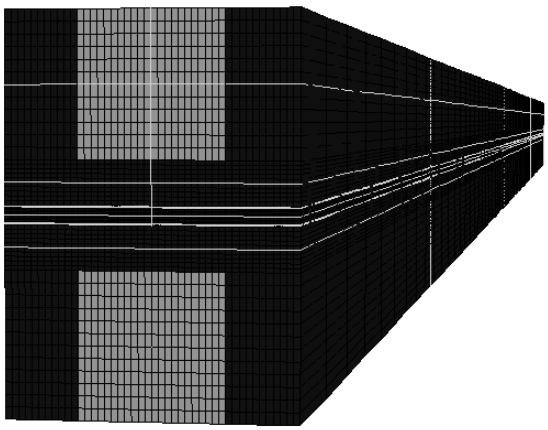

Fig. 3. 3D structured grid of PEMFC

3. MODEL ASSUMPTIONS

The present model includes some assumptions such as: All gases are assumed to be ideal gas mixture, GDLs and catalyst layers are homogeneous porous, flow is incompressible and laminar, because the pressure gradients and velocities are small and the volume of liquid-phase water in the domain is negligible, so the flow field is single phase.

4. GOVERNING EQUATIONS

In this numerical simulation, a single domain model formation was used for the governing equations. These governing equations consist of mass conservation, momentum and species equations, which can be written as:

$$\left(\nabla . \rho \mathbf{u}\right) = 0 \tag{1}$$

$$\frac{1}{\left(\varepsilon^{eff}\right)^2}\nabla.\left(\rho\mathbf{u}\,\mathbf{u}\right) = -\nabla P + \nabla.\left(\mu\nabla\mathbf{u}\right) + S_u \tag{2}$$

$$\nabla.\left(\mathbf{u}\,C_K\right) = \nabla.\left(D_K^{eff}\nabla C_K\right) + S_K \tag{3}$$

$$\nabla.\left(\kappa_e^{eff}\nabla\Phi_e\right) + S_\Phi = 0 \tag{4}$$

In Eq. (1) ρ is the density of gas mixture. According to model assumption, mass source and sink term are neglected. $\mathcal{E}$ is the effective porosity inside porous mediums, and μ is the viscosity of the gas mixture in the momentum equation shown as Eq. (2) The momentum source term, S_u, is used to describe Darcy's drag for flow through porous gas diffusion layers and catalyst layers [24] as:

$$S_u = -\frac{\mu}{K}\mathbf{u} \tag{5}$$

K is the gas permeability inside porous mediums. D_K^{eff} in the species equation as shown in Eq. (3), is the effective diffusion coefficient of species k (e.g. hydrogen, oxygen, nitrogen and water vapor) and is defined to describe the effects of porosity in the porous gas diffusion and catalyst layers by the Bruggeman [25] correlation as:

$$D_K^{eff} = \left(\varepsilon^{eff}\right)^{1.5} D_K \tag{6}$$

Additionally, diffusion coefficient is function of temperature and pressure [26] by the next equation:

$$D_K = D^{\circ}{}_K\left(\frac{T}{T_\circ}\right)^{\frac{3}{2}}\left(\frac{P_\circ}{P}\right) \tag{7}$$

Transport properties for species are given in Table 1.

Table 1. Transport properties [26]

Property	Value
H_2 Diffusivity in the gas channel, D^0_{H2}	1.10×10^{-04} m^2/s
O_2 Diffusivity in the gas channel, D^0_{o2}	3.20×10^{-05} m^2/s
H_2O Diffusivity in the gas channel, D^0_{H2o}	7.35×10^{-05} m^2/s
H_2 Diffusivity in the membrane, D^{mem}_{H2}	2.59×10^{-10} m^2/s
O_2 Diffusivity in the membrane, D^{mem}_{o2}	1.22×10^{-10} m^2/s

The charge conservation equation is shown as Eq. (4) and κ_e is the ionic conductivity in the ion metric phase and has been incorporated by Springer, Zawodzinski, and Gottesfeld [27] as:

$$k_e = \exp\left[1268\left(\frac{1}{303}-\frac{1}{T}\right)\right]\times(0.005139\lambda - 0.00326) \tag{8}$$

Moreover, in the above equation, λ is defined as the number of water molecules per sulfonate group inside the membrane. The water content can be assumed as a function of water activity, a is defined according to the experimental data [28]:

$$\lambda = 0.3+6a\left[1-\tanh\left(a-0.5\right)\right]+3.9\sqrt{a}\left[1+\tanh\left(\frac{a-0.89}{0.23}\right)\right] \tag{9}$$

Water activity a is defined by:

$$a = \frac{C_w R T}{P_w^{sat}} \tag{10}$$

The proton conductivity in the catalyst layers by introducing the Bruggeman correlation [29] can be given by:

$$\kappa_e^{eff} = \varepsilon_m^{1.5} \kappa_e \tag{11}$$

In the above equation ε_m is the volume fraction of the membrane-phase in the catalyst layer. The source and sink term in Eqs. (3) and (4) are presented in Table 2. Local current density in the membrane can be calculated by:

$$I = -\kappa_e \nabla \Phi_e \tag{12}$$

Then the average current density is calculated as follows:

$$I_{ave} = \frac{1}{A} \int_{A_{mem}} I dA \tag{13}$$

Where, A is the active area over the MEA.

Table 2. Source/sink term for momentum, species and charge conservation equations for individual regions

	Momentum	Species	Charge
Flow channels	$S_u = 0$	$S_K = 0$	$S_\Phi = 0$
Bipolar plates	$S_u = -\frac{\mu}{K}\mathbf{u}$	$S_K = 0$	$S_\Phi = 0$
GDLs	$S_u = -\frac{\mu}{K}\mathbf{u}$	$S_K = 0$	$S_\Phi = 0$
Catalyst layers	$S_u = 0$	$S_K = -\nabla.\left(\frac{n_d}{F} I\right) - \frac{S_{K,}}{nF}$	$S_\Phi = j$
Membrane	$S_u = 0$	$S_K = -\nabla.\left(\frac{n_d}{F} I\right)$	$S_\Phi = 0$

5. WATER TRANSPORT

Water molecules in PEM fuel cell are transported via electro-osmotic drag due to the properties of polymer electrolyte membrane in addition to the molecular diffusion. H^+ protons transport water molecules through the polymer electrolyte membrane and this transport phenomenon is called electro-osmotic drag. In addition to the molecular diffusion and electro-osmotic drag, water vapor is also produced in the catalyst layers due to the oxygen reduction reaction.

Water transport through the polymer electrolyte membrane is defined by:

$$\nabla . \left(D_{H_2O}^{mem} \nabla C_{H_2O}^{mem} \right) - \nabla . \left(\frac{n_d}{F} \boldsymbol{i} \right) = 0 \tag{14}$$

where n_d and $D_{H_2O}^{mem}$ are defined as the water drag coefficient from anode to cathode and the diffusion coefficient of water in the membrane phase, respectively.

The number of water molecules transported by each hydrogen proton H^+ is called the water drag coefficient. It can be determined from the following equation [28]:

$$n_d = \begin{cases} 1 & \lambda < 9 \\ 0.117\lambda - 0.0544 & \lambda \geq 9 \end{cases} \tag{15}$$

The diffusion coefficient of water in the polymer membrane is dependent on the water content of the membrane and is obtained by the following fits of the experimental expression [30]:

$$D_w^{mem} = \begin{cases} 3.1\times10^{-7}\,\lambda\left(e^{0.25\lambda}-1\right)e^{\left(\frac{-2346}{T}\right)} & 0<\lambda\leq 3 \\ 4.17\times10^{-8}\,\lambda\left(1+161e^{-\lambda}\right)e^{\left(\frac{2346}{T}\right)} & otherwise \end{cases} \tag{16}$$

The terms are therefore related to the transfer current through the solid conductive materials and the membrane. The transfer currents or source terms are non-zero only inside the catalyst layers. The transfer current at anode and cathode can be described by Tafel equations as follows:

$$R_{an} = j_{an}^{ref}\left(\frac{[H_2]}{[H_2]_{ref}}\right)^{\gamma an}\left(e^{\alpha_{am}F\eta_{an}/RT} - e^{-\alpha_{cat}F\eta^{an}/RT}\right) \tag{17}$$

$$R_{cat} = j_{an}^{ref}\left(\frac{[O_2]}{[O_2]_{ref}}\right)^{\gamma cat}\left(-e^{\alpha_{am}F\eta_{cat}/RT} + e^{-\alpha_{cat}F\eta^{cat}/RT}\right) \tag{18}$$

According to the Tafel equation, the current densities in the anode and cathode catalysts can be expressed by the exchange current density, reactant concentration, temperature and over-potentials. The surface over potential is defined as the difference between proton potential and electron potential.

$$\eta_{an} = \phi_{sol} - \phi_{mem} \tag{19}$$

$$\eta_{cat} = \phi_{sol} - \phi_{mem} - V_{oc} \tag{20}$$

The open circuit potential at the anode is assumed to be zero, while the open circuit potential at the cathode becomes a function of a temperature as:

$$V_{oc} = 0.0025T + 0.2329 \tag{21}$$

The protonic conductivity of membrane is dependent on water content, where σ_m is the ionic conductivity in the ionomeric phase and has been correlated by Springer, Zawodinski and Gottesfeld [31]:

$$\sigma_{\mathrm{m}} = (0.005139\lambda - 0.00326)\exp\left[1268\left(\frac{1}{303} - \frac{1}{\mathrm{T}}\right)\right] \tag{22}$$

Energy equation given by Eq. (23):

$$\nabla.(\rho\,\mathbf{u}\,\mathrm{T}) = \nabla.(\lambda_{\mathrm{eff}}\nabla\,\mathrm{T}) + \mathrm{s}_{\mathrm{T}} \tag{23}$$

Where, λ_{eff} is the effective thermal conductivity and the source term of the energy equation, S_T, is defined with the following equation:

$$S_T = I^2R_{ohm} + h_{reaction} + \eta_a i_a + \eta_c i_c \tag{24}$$

In this equation, R_{ohm} is the ohmic resistance of the membrane, $h_{reaction}$ is the heat generated through the chemical reactions, and η_a and η_c are the anode and cathode overpotentials which are calculated as:

$$R_{ohm} = \frac{t_m}{\sigma_e} \tag{25}$$

Here, t_m is the membrane thickness.

$$\eta_a = \frac{RT}{\alpha_a F} \ln\left[\frac{IP}{j_{0_a} P_{0_{H_2}}}\right] \tag{26}$$

$$\eta_C = \frac{RT}{\alpha_c F} \ln\left[\frac{IP}{j_{0_c} P_{0_{O_2}}}\right] \tag{27}$$

Where, α_a and α_c are the anode and cathode transfer coefficients, $P_{0_{H_2}}$, $P_{0_{O_2}}$ is the partial pressure of hydrogen and oxygen respectively, and j_0 is the reference exchange current density. The fuel and oxidant fuel rate $\mathbf{u}$ is given by the following equations:

$$\begin{aligned} \mathbf{u}_{in,a} &= \frac{\xi_a I_{ref} A_{mem}}{2 C_{H_2,in} F A_{ch}} \\ \mathbf{u}_{in,c} &= \frac{\xi_c I_{ref} A_{mem}}{4 C_{O_2,in} F A_{ch}} \end{aligned} \tag{28}$$

In the above equations, I_{ref} and ξ are the reference current density and stoichiometric ratio, respectively. ξ is defined as the ratio between the amount of fuel supplied and the amount of fuel required based on the reference current density. The species concentrations of flow inlets are assigned by the humidification conditions of both the anode and cathode inlets.

6. BOUNDARY CONDITION

Equations (1) to (4) form the complete set of governing equations for the traditional mathematical model. Boundary conditions are dispensed at the external boundaries. Constant mass flow rate at the channel inlet and constant pressure condition at the channel outlet are assumed and the no-flux conditions are executed for mass, momentum, species and potential conservation equations at all boundaries except for inlets and outlets of the anode and cathode flow channels.

7. RESULTS AND DISCUSSION

a) Model validation

A series of simulations were carried out on the model from low to high operating current densities. In order to evaluate the validity of the model, numerical simulation results were compared with the experimental data presented by Wang et al [32], as shown in Fig. 4, in which there is a favorable agreement between them. The power density curve for the model is illustrated too. As we know, there is a relation between voltage, current density and the power of the fuel cell as P=V*I. Fuel cell operating condition and geometric parameters are shown in Table 3. A fully humidified inlet condition is used for the anode and cathode.

In this work the operation and performance of a single straight cell as mentioned above, in two different cell voltages was studied and compared.

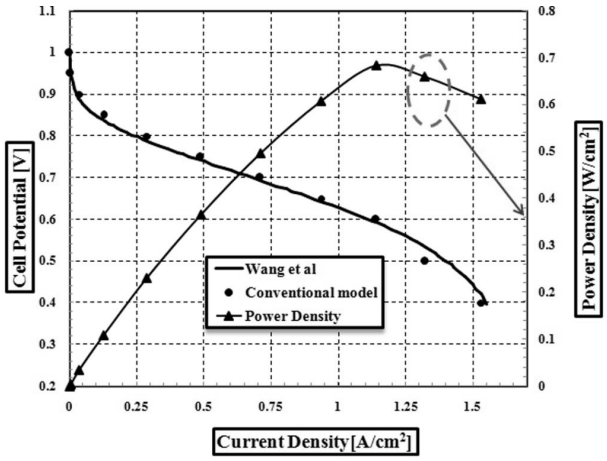

Fig. 4. Comparison of polarization curve of model with experimental data and power density curve at 1.5 (A/m^2)

Table 3. Geometrical parameters and operating conditions [32]

Parameter	Value
Gas channel length	7.0×10^{-2} m
Gas channel width and depth	1.0×10^{-3} m
Bipolar plate width	5.0×10^{-4} m
Gas diffusion layer thickness	3.0×10^{-4} m
Catalyst layer thickness	1.29×10^{-5} m
Membrane thickness	1.08×10^{-4} m
Cell temperature	70^0 C
Anode pressure	3 atm
Cathode pressure	3 atm

Figure 5 illustrates the distribution of oxygen mass fraction at membrane-cathode catalyst layer interface. Lack of oxygen at the shoulder region at the top of the reacting area conduces to higher mass fraction losses. For the downstream region of the channel, higher mass fraction losses become worse due to diminution of the reactant with moving downstream. As shown in Fig. 6, when the cell voltage increases, the cell current density decreases, hence there is a reduction in oxygen consumption due to the general increase in the mass fraction of oxygen. Figures 7a, 7b display the oxygen mass fraction contour of a cathode catalyst layer at 0.6V, 0.7V. Both figures show oxygen mass fraction decreases along the flow channel due to the consumption of oxygen at the catalyst layer. At the catalyst layer, the concentration of oxygen is balanced by consuming the oxygen and the amount of oxygen that diffuses towards the catalyst layer, driven by the concentration gradient. The lower diffusivity of the oxygen along the flow with the low concentration of oxygen in ambient air results in noticeable oxygen diminution along the cell. At higher cell voltages, the rate of oxygen consumption is low enough that it does not cause any diffusive problems, whereas at a low cell voltage the concentration of oxygen has already reached near-zero values. Low diffusivity of the hydrogen is similar to the oxygen. Figure 8a, 8b display the variation of mass fraction of hydrogen along the anode catalyst at different cell voltages. The hydrogen mass fraction decreases along the cell as it is being consumed. However, the decrease in mass fraction of the hydrogen along the anode side is smaller than that for the oxygen in cathode side due to the higher diffusivity of the hydrogen.

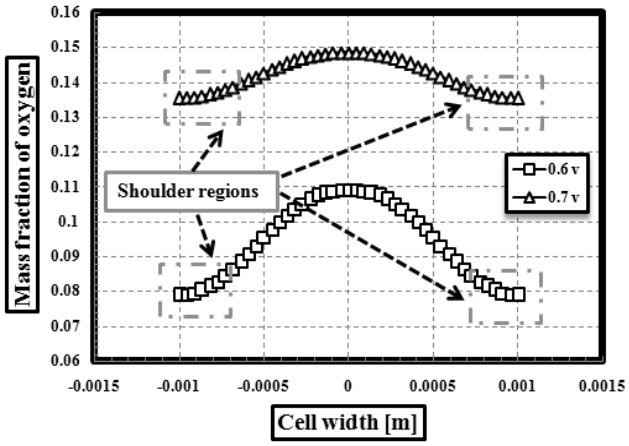

Fig. 5. Oxygen mass fraction at membrane-cathode GDL interface for two different cell voltages at L/L_0=0.1428 (entry region)

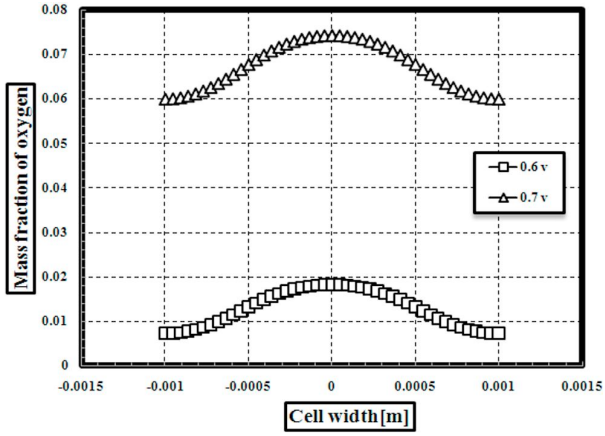

Fig. 6. Oxygen mass fraction at membrane-cathode GDL interface for two different cell voltages at L/L_0=0.8571(exit region)

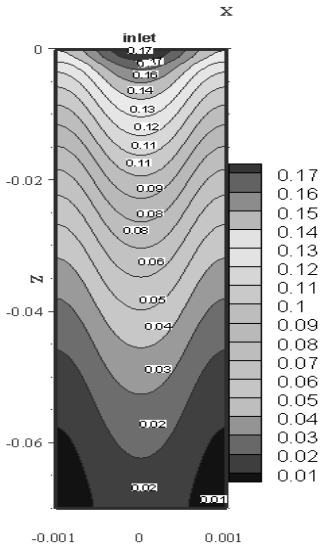

Fig. 7a. Mass fraction of oxygen at cathode catalyst (0.6V)

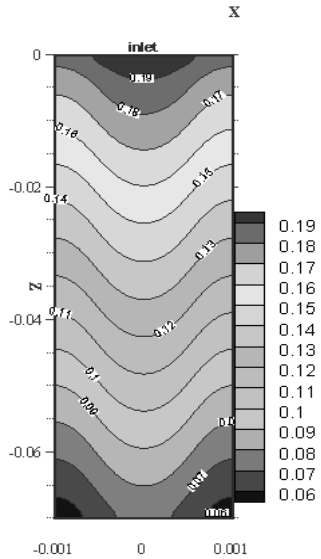

Fig. 7b. Mass fraction of oxygen at cathode catalyst (0.7V)

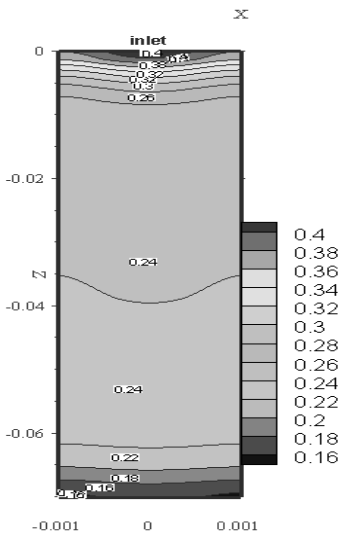

Fig. 8a. Mass fraction of hydrogen at anode catalyst (0.6V)

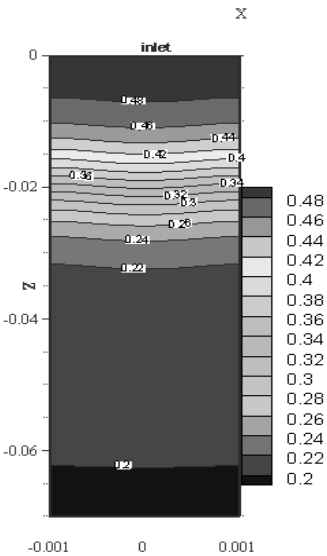

Fig. 8b. Mass fraction of hydrogen at anode catalyst (0.7V)

Hydrogen at the anode produces a proton, releasing an electron in the process that must pass through an external circuit to reach the cathode. The proton, which remains solvated with a certain number of water molecules, diffuses through the membrane to the cathode to react with oxygen and the returning electron. Water is produced at the cathode. Variation of the water mass fraction, fully humidified along the fuel cell is shown in Figs. 10 and 11 for 0.6V and 0.7V respectively.

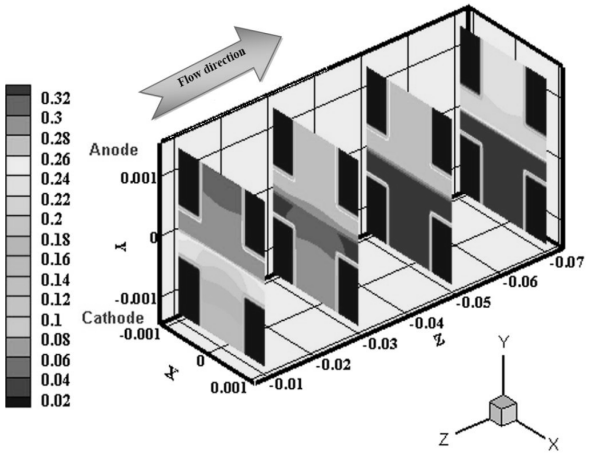

Fig. 9. Variance of water mass fraction (0.6V)

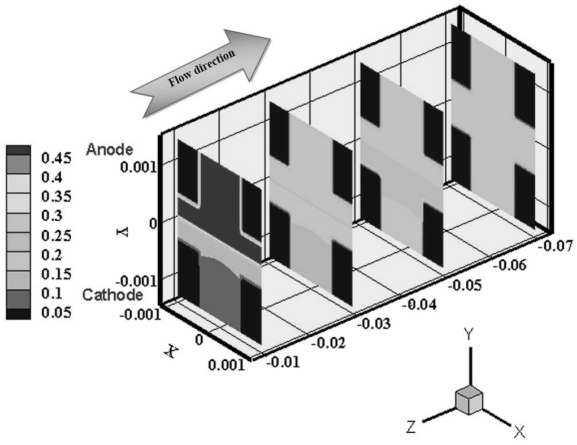

Fig. 10. Variance of water mass fraction (0.7V)

The magnitude of water mass fractions is higher for low cell voltage than for high cell voltage. The back diffusion is sufficient to counteract the electro-osmotic drag, but under low voltage, the electro-osmotic effect dominates back diffusion. Water concentration at the cathode channel increases along the flow channel. This increase of water concentration is associated with the phenomenon that the water is composed by electrochemical reaction along the channel and water is transported from the anode side by electro-osmotic drag coincidently.

Water activity depends on concentration of water in both anode and cathode sides. Therefore, at the cathode side the concentration of water increases along the flow channel, hence water activity increases along the flow channel at the cathode side. Figures 11, 12 display water activity at the membrane-cathode GDL interface for 0.6V, 0.7V respectively.

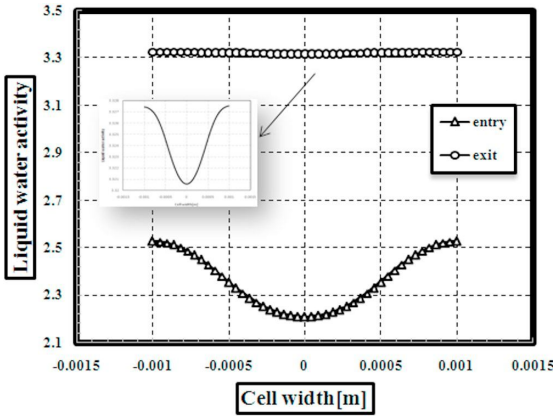

Fig. 11. Liquid water activity at membrane-cathode catalyst interface.(entry region, L/L_0= 0.1428) ,(exit region, L/L_0=0.8571) , at 0.6V

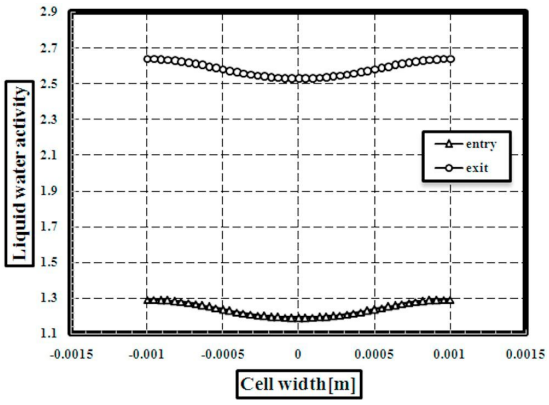

Fig. 12. Liquid water activity at membrane-cathode catalyst interface.(entry region, L/L0= 0.1428) ,(exit region, L/L0=0.8571), at 0.7V

Protonic conductivity is one of the main parameters for proton exchange membrane (PEMFC) which contributes to the fuel cell performance in terms of ohmic loss. Comparisons of the protonic conductivity in both voltages are shown in Figs. 13 and 14; high protonic conductivity is necessary to support high

currents with minimal resistive losses. The protonic conductivity is highly influenced by the water content. Membrane conductivity is a function of water activity. Increasing the water activity along the channel leads to increasing conductivity, also reducing the length of the proton transport path leads to proton conductivity increase.

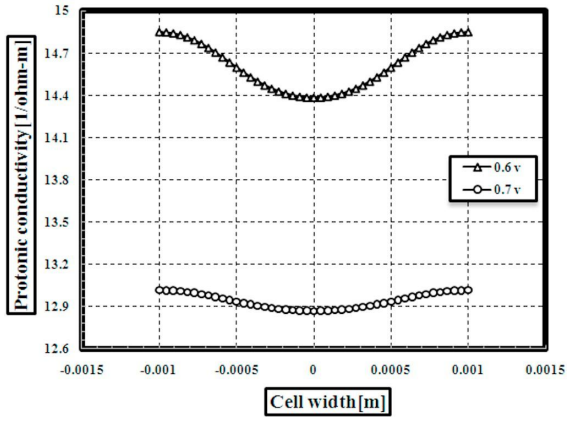

Fig. 13. Protonic conductivity at membrane-cathode catalyst interface (entry region, L/L0=0.1428)

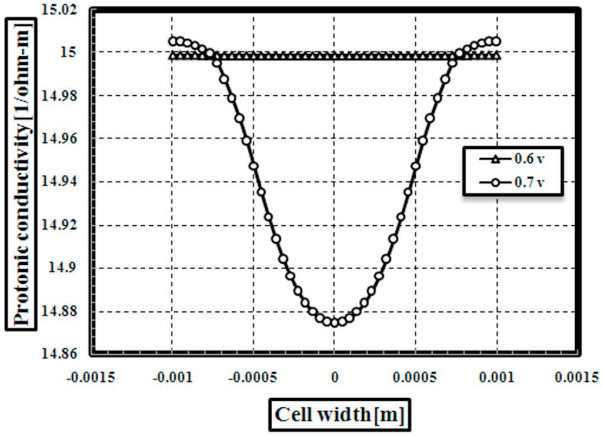

Fig. 14. Protonic conductivity at membrane-cathode catalyst interface (exit region, L/L0=0.8571)

8. CONCLUSION

A three dimensional, computational fluid dynamic model of a PEM fuel cell with straight flow channels was developed. The simulated results include the polarization curve, the power density, and the oxygen and hydrogen mass fraction distribution in the cathode and anode respectively, and water activity and protonic conductivity in the PEMFC. In this numerical simulation good agreement between the numerical result and the experimental data was shown. Transport phenomena such as curves and contours of mass fraction of species and liquid water activity and protonic conductivity for two different cell voltages (0.6V, 0.7V) were compared. Whenever cell voltage increases, corresponding current density decreases and variation of mass fraction of species in the entry region and exit region of the cell is noticeable.

NOMENCLATURE

a	water activity
C	molar concentration [mol/m^3]
D	mass diffusion coefficient [m^2/s]
F	faraday constant [C/mol]
I	local current density [A/m^2]
J	exchange current density [A/m^2]
K	permeability [m^2]
M	molecular weight [kg/mol]
n_d	electro-osmotic drag coefficient
P	pressure [Pa]
R	universal gas constant [J mol^{-1} K^{-1}]
T	temperature [K]
t	thickness
$\vec{u}$	velocity vector
V_{cell}	cell voltage
V_{oc}	open-circuit voltage
W	width
X	mole fraction
A_s	specific area of catalyst layer (m^{-1})

Greek letters

α	water transfer coefficient
ε^{eff}	effective porosity
ρ	density [kg/m^3]
ϕ_e	electrolyte phase potential [v]
μ	viscosity [kg m^{-1}s^{-1}]
σ_e	membrane conductivity [1.ohm^{-1}m^{-1}]
λ	water content in the membrane
ζ	stoichiometric ratio
η	over potential [v]
λ_{eff}	effective thermal conductivity [w m^{-1}k^{-1}]

Subscripts and superscripts

a	anode
c	cathode
ch	channel
k	chemical species
m	memberane
MEA	memberane electrolyte assembly
ref	reference value
sat	saturated
w	water

REFERENCES

1. Kazim, A., Liu, H. T. & Forges, P. (1999). Modeling of performance of PEM fuel cells with conventional and interdigitated flow fields. *J. Appl.Electrochem.*, Vol. 29, pp. 1409–1416.
2. Nguyen, T. V. (1999). Modeling two-phase flow in the porous electrodes of proton exchange membrane fuel cells using the interdigitated flow fields. Presented at the *195th Meeting of Electrochemical Society*, Seattle.
3. Wood, D. L., Yi, J. S. & Nguyen, T. V. (1998). Effect of direct liquid water injection and interdigitated flow field on the performance of proton exchange membrane fuel cells. *Electrochem*, Vol. 43, pp. 3795–3809.
4. Farhangi, S., Mostafavi, M. & Poursoltani, A. (2005). Development of a stand-alone lighting system for 70 W hps lamps. *Iranian Journal of Science & Technology, Transaction B:* Engineering, Vol. 26, No. B4, pp. 687-692.
5. Grujicic, M., & Chittajallu, K. M. (2004). Design and optimization of polymer electrolyte membrane (PEM) fuel cells. *Applied Surface Science*, Vol. 227, pp. 56–72.
6. Xing et al. (2010). Optimization of assembly clamping pressure on performance of proton-exchange membrane fuel cells. *J. Power Sources*, Vol. 195, pp. 62-68.
7. Chang et al. (2007). Effect of clamping pressure on the performance on a PEM fuel cell. *J. Power Sources*, Vol. 166,
8. pp. 149-154.
9. Rho, Y. W., Velev, O. A., Srinivasan, S., Kho, Y. T. (1994). Mass transport in proton exchange membrane fuel cells using O2/H2, O2/Ar, and O2/N2 mixtures. *J. Electrochem. Soc.*, Vol. 141, p. 3838.
10. Amphlett, J. C., Baumert, R. M., Mann, R. F., Peppley, B. A., Roberge, P. R. & Harris, T. J. (1995). Performance modeling of the Ballard Mark IV solid polymer electrolyte fuel cell. I. Mechanistic model development, *J. Electrochem. Soc.*, Vol. 142, p. 9.
11. Mosdale, R. & Srinivasan, S. (1995). Analysis of performance and of water management in proton exchange membrane fuel cells, *Electrochem. Acta*, Vol. 40, pp. 413-421.

12. Oetjen, H. F., Schmidt, V. M., Stimming, U. & Trila, F. (1996). Performance data of a proton exchange membrane fuel cell using H2/Co as fuel gas, *J. Electrochem.Soc*., Vol. 143, p. 3838.
13. Büchi, F. N. & Srinivasan, D. (1997). Operating proton exchange membrane fuel cells without external humidification of the reactant gases. *J. Electroc*hem. *Soc*., Vol. 144, p. 2767.
14. Uribe, F. A., Gottesfeld, S. & Zawodzinski, T. A. (2002). Effect of ammonia as potential fuel impurity on proton exchange membrane fuel cell performance. *J. Electrochem.* Soc., Vol. 149, A293–A296.
15. Ticianelli, E. A., Derouin, C. R. & Srinivasan, S. Localization of platinum in low catalyst loading electrodes to attain high power densities in SPE fuel cells. *J. Electro anal. Chem*., Vol. 251, p. 275.
16. Yao, K. Z., Karan, K., McAuley, K. B., Oosthuizen, P., Peppley, B. & Xie, T. (2004). A review of mathematical models for hydrogen and direct methanol polymer electrolyte membrane fuel cells. *Fuel Cells* 4 (1/2), pp. 3–29.
17. Natarajan, D., Nguyen, T. V. (2001). A two-dimensional, two-phase, multi component, transient model for the cathode of a proton exchange membrane fuel cell using conventional gas distributors. *J. Electrochem. Soc*. Vol. 148, No. 12, A1324–A1335.
18. Lin, G. & Nguyen, T. V. (2006). A two-dimensional two-phase model of a PEM fuel cell. *J. Electrochem. Soc*., Vol. 153, No. 2, A372–A382.
19. Lum, K. W. & McGuirk, J. J. (2005). Three-dimensional model of a complete polymer electrolyte membrane fuel cell – model formulation, validation and parametric studies, *J. Power Sour*. , Vol. 143, pp. 103–124.
20. Ahmed, D. H., Sung, H. J. (2006). Effects of channel geometrical configuration and shoulder width on PEMFC performance at high current density. *Power Sour*., Vol. 162, pp. 327–339.
21. Majidifar, S., Mirzaei, I., Rezazadeh, S., Mohajeri, P. & Oryani, H. (2011). Effect of gas channel geometry on performance of PEM fuel cells. *Australian Journal of Basic and Applied Sciences*, Vol. 5, No. 5, pp. 943-954.
22. Pourmahmoud, N., Rezazadeh, S., Mirzaee, I. & Heidarpoor, V. (2011). Three-dimensional numerical analysis of proton exchange membrane fuel cell. *Journal of Mechanical Science and Technology* (JMST), Vol. 25, No. 10, pp. 2665-2673.
23. Ahmadi, N., Pourmahmoud, N., Mirzaee, I. & Rezazadeh, S. (2011). Three-dimensional computational fluid dynamic study of effect of different channel and shoulder geometries on cell performance. *Australian Journal of Basic and Applied Sciences*, Vol. 5, No. 12, pp. 541-556.
24. Ahmed, D. H., Sung, H. J. (2008). Design of a deflected membrane electrode assembly for PEMFCs. Int. *J. Heat and Mass Transfer*, Vol. 51, pp. 5443–5453.
25. Garau, V., Liu, H. & Kakac, S. (1998). *AIChE J*., Vol. 44, No. 11, pp. 2410-2422.
26. Meredith, R. E. & Tobias, C. W. (1991). *Advances in electrochemistry and electrochemical engineering 2*. Tobias,C.W., ed., *Interscience Publishers*, New York.
27. Byron Bird, R., Stewart, W. E. & Edwin, N. (1960). Lightfoot, in *Transport Phenomena*. John Wiley & Sons, Inc.
28. Springer, T. E., Zawodzinski, T. A. & Gottesfeld, S. (1991). *J. Electrochem.* Soc. Vol. 138, pp. 2334-2342.
29. Kuklikovsky, A. A. (2003). *J. Electrochem. Soc.*, Vol. 150, No. 11, A1432-A1439.
30. Meredith, R. E. & Tobias, C. W. (1960). *Advances in electrochemistry and electrochemical engineering.* Tobias, C.W., ed., Interscience Publishers, New York.
31. Yeo, S. W. & Eisenberg, A. (1997). *J. Appl. Polym. Sci*., Vol. 21, p. 875.
32. Springer, T. E., Zawodinski, T. A. & Gottesfeld, S. (1991). *J. Electrochem. Soc.*, Vol. 136, p. 2334.
33. Wang, L., Husar, A., Zhou, T. & Liu, H. (2003). *Int. J. Hydrog. Energy*, Vol. 28, No. 11, pp. 1263-1272.